

Dissociation of multiply charged ICN by Coulomb explosion

J.H.D. Eland^{1,2}, R. Singh², J.D. Pickering³, C.S. Slater^{2,3}, A. Hult Roos², J. Andersson², S. Zagorodskikh^{2,4}, R.J. Squibb², M. Brouard³, and R. Feifel²

¹*Department of Chemistry, Physical and Theoretical Chemistry Laboratory, Oxford University, South Parks Road, Oxford OX1 3QZ, United Kingdom*

²*Department of Physics, University of Gothenburg, Origovägen 6B, SE-412 96 Gothenburg, Sweden*

³*Department of Chemistry, The Chemistry Research Laboratory, Oxford University, Mansfield Road, Oxford OX1 3TA, United Kingdom*

⁴*Department of Physics and Astronomy, Uppsala University, Box 516, SE-751 20 Uppsala, Sweden*

Abstract

The fragmentations of iodine cyanide ions created with 2 to 8 positive charges by photoionization from inner shells with binding energies from 59 eV (I 4d) to ca. 900 eV (I 3p) have been examined by multi-electron and multi-ion coincidence spectroscopy with velocity map imaging (VMI) ion capability. The charge distributions produced by hole formation in each shell are characterised and systematic effects of the number of charges and of initial charge localisation are found.

Introduction

Multiply charged molecular ions, however created, dissociate rapidly into charged and neutral fragments as a result of bonding electron loss and of Coulomb repulsion between the charges. It is often assumed, ever since the term “Coulomb explosion” was coined [1], that after a sufficiently energetic ionization event a molecule is completely atomised and all the atomic products are charged. If only Coulomb forces operate (which is not always true [2]), this assumption allows molecular structures and even absolute stereochemistry to be deduced from the measured momentum vectors of the product ions [3-5]. But the validity of the basic assumption has never been tested directly. Questions which arise include: are there really no molecular or neutral products?; does the breakup happen in a single step or in successive steps?; what determines which fragments are multiply charged and which singly charged?; what roles are played by charge transfer or by location of the initial charge on a particular atom? We have begun a programme in which the detailed outcome of real molecular Coulomb explosions is to be studied under a range of conditions to address such questions, particularly as a function of the ratio of number of charges to the number of atoms. As a first hypothesis we assume that for a given molecule the number of charges is the most important determinant of the final outcome, although it is clear that there will be other factors such as the amount of internal energy initially deposited in the ions and the time sequence of energy deposition and charge transfer. In this initial work, we examine triatomic ICN, and induce different charge states by inner-shell ionization. The identity of the initial hole state is monitored by coincident electron spectroscopy while the final outcome is monitored by multi-particle mass spectrometry and velocity map imaging (VMI), also in coincidence.

The ICN molecule is linear in its ground state, with a relatively long I-C bond (199.5 pm) and a much shorter C-N bond (115.9 pm). Although the molecule is linear when averaged over time, at any instant it is most likely to be bent because of zero-point energy in the degenerate bending

vibration. The double ionization spectrum and the dissociation of doubly charged ICN have been investigated before by related low-energy coincidence techniques [6,7] providing a useful starting point for the present work. The dissociation of ICN cations after photoionization at energies above the I 4d and 3d thresholds has also been examined by an ion-ion coincidence technique [8]. That work showed that up to 7-fold ionisation is produced by I 3d hole formation, but indicated that the overall the dissociation dynamics are not fully explained by pure Coulomb explosion.

Experimental methods

Experiments were carried out using energy-selected synchrotron radiation provided at beamlines U49/2-PGM-2 and U52-SGM in separate experimental runs at the BESSY II storage ring of the Helmholtz Zentrum Berlin, operating in single bunch mode. Because the light pulse repetition rate in this mode (1.25 MHz) is much too high for our mass spectrometer, the rate was reduced to 10 kHz by a synchronous chopper [9]. The sub-nanosecond pulses of light meet an effusive jet of target gas in the source region of the apparatus shown in Fig. 1, which has been described before [10]. In contrast to the work described there, the apparatus was operated for the present work in VMI mode [11], capturing images of the ion spatial distributions at the delay-line position-sensitive detector [12]. The electrode arrangement is carefully devised to provide cylindrically symmetric electric fields, but because a strong permanent magnetic field is essential in the source to capture electrons, the early ion trajectories are significantly distorted. Compensating magnets are placed as near as possible to the source region to undo the majority of the distortion without affecting electron resolution. The compensation brings all but the lightest (H^+ , He^+) thermal ions safely back to the centre of the detector, but a small (ca. 10 %) distortion of the rings for energetic ions into ovals remains. This residual distortion is corrected by an axis transformation in the data analysis.

The performance of the magnetic bottle time-of-flight (TOF) electron spectrometer in this apparatus is slightly compromised by the greater distance (ca. 10 mm) between the conical magnet and the ionization zone, as compared with operation for electrons only (ca. 2 mm distance). The magnetic field at the interaction point is thereby reduced to a few hundred Gauss and the numerical resolution $E/\Delta E$ is about 30 rather than 50 or 60, but this is still sufficient, with astute choice of photon energy, to isolate all the individual photoelectron lines of interest. The electron collection efficiency remains high. The mass spectrometer is a two-field TOF mass selector working with potentials optimised for VMI operation using a delay-line anode (RoentDek HEX80) for position sensitivity. For technical reasons the kinetic energy of ions hitting the microchannel plate detector was limited to 2 keV in the runs at beamline U49/2-PGM-2 but was raised to 4 keV for the runs at U52-SGM. At the lower ion energy there was marked discrimination against heavy ions which could be quantified only approximately; for this reason we present data from the two sets of runs separately. Some of the lighter ions produced by Coulomb explosions have high initial kinetic energies which distort their flight time distributions and reduce their effective collection efficiencies because high transverse velocities prevent them from reaching the sensitive area of the detector. For these reasons the relative intensities of different processes tabulated in this paper are reliably characteristic of trends in the ion breakdown behaviour, but are not to be taken as accurate total proportions.

Results

Electron-ion coincidence measurements were made at six photon energies, 110, 135, 200, 640, 945 and 1200 eV at beamline U49/2-PGM-2 and at four further energies, 350, 450, 700 and 1040 eV at

beamline U52-SGM. These energies span the range where single holes can be created in the following inner shells, in order of binding energy: I 4d (59.2, 60.8 eV), I 4p (132 eV), I 4s (194 eV), C 1s (295 eV), N 1s (400 eV), I 3d (632, 643 eV), I 3p (885, 940 eV). These measured binding energies for ICN are all about 10 eV higher than values given for elemental iodine in reference tables. At each photon energy the coincident electron spectrum allows us to identify events in which individual inner shell holes are created. The first results are the overall mass spectra produced by single vacancy creation in each inner shell. The extraction of these spectra requires careful subtraction of accidental false coincidences and of continuum background underlying the photolines, which is particularly important for the weak photoelectron lines such as I 4s. This has been done by subtracting mass spectra extracted from regions of the electron spectra of the same width as the photoelectron lines and immediately adjacent to them. The spectra from the separate runs are presented in Figs. 2 and 3. Because electrons are best resolved at low energy, the electron spectra used for photoelectron line selection are generally those taken at the lowest photon energy above each shell where the cross-section is sufficient. The iodine s-shells have low cross-sections at all energies and the 4s shell is the only one that could be selected effectively, at 350 eV photon energy. For iodine 3p the intensity at 945 eV is also low, perhaps because of a Cooper minimum, and $3d^{-1}$ ionization is dominant. The two levels of the 3p shell are seen clearly at 1040 eV and 1200 eV photon energy.

The mass spectra induced by iodine inner-shell ionization in Figs. 2 and 3 show increasing degrees of ionization when deeper shells are broached. As the intensities of more highly ionized atoms rise, the less ionized atoms and the molecular fragments CN^+ and IC^+ disappear. Carbon and nitrogen dications appear already after I 4p hole formation, but C^{3+} and N^{3+} appear only very weakly after creation of the deepest inner-shell hole in I 3p, despite being energetically accessible at lower energy. Nitrogen ions always appear to be less abundant in the spectra than C ions. This is at least partly because the N^{n+} ions invariably have higher kinetic energy releases than the carbon ions, as shown by both the hollowness of their TOF peak shapes and by the spillage of the N^{n+} ions off the sensitive area of the detector. The loss of sensitivity for nitrogen ions is severe especially when the other ions produced in the same events are highly charged. Carbon ions are subject to similar losses to a lesser extent. With formation of deeper inner-shell holes on the iodine atom starting with $4p^{-1}$, Auger cascades become not only possible but dominant, and lead to higher degrees of ionisation. The mass spectra change abruptly as I^+ and CN^+ vanish and more highly charged iodine ions appear.

Besides the mass spectra, we can also examine ion-ion-electron and ion-ion-ion-electron coincidences, again with careful subtraction of accidental coincidences and of continuum and other interfering background. A special advantage of using a triatomic target like ICN is that when three atomic ions are detected in coincidence, all atoms have been accounted for and there can be no neutral fragments to complicate the analysis. We now consider each initial hole state in turn, roughly in order of the extent of ionization produced.

Iodine $4d^{-1}$

The binding energy of the 4d shell in ICN near 60 eV is above the double and triple ionization energies of ICN (28.5 eV and ca. 55 eV) but below both the estimated fourfold molecular ionization threshold of 90 eV and the thermodynamic threshold for fourfold ionized fragments ($I^{2+} + C^+ + N^+$, 66.3 eV). So only double and triple ionization can occur in coincidence with the 4d photoelectrons. Because the 4d energy is close to the triple ionization threshold, few levels of the triply charged ion can be populated. For each triply charged level the phase space available for direct double Auger

decay increases linearly with energy above the threshold, so for these two reasons the proportion of triple ionization is expected to be small. In order to evaluate the fractions of different ion pairs created after formation of a 4d vacancy we calculate ion-ion coincidence maps or arrays, simultaneously coincident in each event with a 4d⁻¹ photoelectron. An isometric projection of the final ion-ion array coincident with 4d is shown as Fig. 4. To leave only true triple (e-i-i) coincidences we first create an array of purely accidental coincidences and subtract it, then carry out exactly the same procedure in coincidence with a section of the continuum background adjacent to the 4d photoelectron line to obtain a background array. The true coincidences shown in Fig. 3 are the result of subtraction of the background array. To find the number of ion triples (fourfold e-i-i-i coincidences) we create similar arrays of ion pairs coincident not only with the relevant photoelectrons but also with an iodine atomic ion. The only ion triple produced by 4d⁻¹ decay is C⁺ + N⁺ + I⁺ so in this case the array has only a single peak and is not shown. From the total counts in each peak together with an estimated collection efficiency for each ion we can estimate the relative intensity of all the decay processes which follow ionization of a 4d electron, with due accounting for the apparent ion pairs which are really components of ion triples where one fragment was not detected. The resulting intensities are listed in Table 1. The collection efficiencies used were those previously determined and used for Xe [10] under the same experimental conditions.

Because of the uncertainty of the collection efficiencies as well as statistical errors these estimates have at least a 20 % uncertainty range, but should be qualitatively correct. They show that after formation of a 4d vacancy, triple ionization makes up only a few percent of the total decay, and within this low-energy triple ionization there is a significant fraction of molecular (diatomic) fragment formation and also formation of neutral fragments. Both fractions are much higher in double ionization, where a majority of the fragmentations produce a neutral atom product. The relative intensities of the different pathways followed after 4d⁻¹ ionization and decay are similar to those produced in double ionization by 48.4 eV photons, where these are known [7].

Nitrogen 1s and carbon 1s holes

The mass spectra produced by C 1s and N 1s photoionization (cf. Fig. 3) do not show a higher degree of ionization, despite the high binding energy (295 and 400 eV) of the initial holes; indeed, they closely resemble the spectrum produced by I 4d ionisation (binding energy 59 eV). The I⁺ ion and molecular CN⁺ remain prominent in the mass spectra. This is easily understood, because no Auger cascades are possible in these atoms but only single, double and to a very minor extent triple Auger decay. Recent measurements [13] confirm that because of the 2-electron and 3-electron nature of double and triple Auger decay, these processes have typical abundances of 10 % and 1 % in carbon and nitrogen 1s-hole decay relative to single Auger. The spectra in Fig. 3 do, however, exhibit interesting charge localisation effects. The IC²⁺ fragment appears prominently when the initial hole is on N or I, but not when it is on the C atom, suggesting that the C—I bond is most likely to be broken when the initial charge is on carbon. The I³⁺ ion appears more strongly after C 1s hole formation than after N 1s ionization suggesting a nearest neighbour effect in the charge transfer from C to I. Fourfold ionization is energetically possible from the 1s hole states, but its extent is negligible because it can be produced only by multi-electron transitions. In practice, the data are insufficient to yield quantitative results for the fourfold coincidences (electron-ion-ion-ion) in this case, as the uncertainty of the background subtraction exceeds the remaining signal. In threefold coincidences (electron-ion-ion) the ratio of CN⁺ + I²⁺ to CN⁺ + I⁺ is the same, within the estimated experimental errors for N 1s as for I 4d initial hole production.

Iodine 4p⁻¹ and 4s⁻¹

With formation of deeper inner-shell holes on the iodine atom starting with 4p⁻¹, Auger cascades become not only possible but dominant, and lead to higher degrees of ionization. The mass spectra change abruptly as I⁺ and CN⁺ vanish and more highly charged iodine ions appear. Although the binding energy of I 4s (194 eV) is higher than that of I 4p (132 eV) there is little apparent difference in the subsequent fragmentation behaviour. Because the cross-section for photoionization from I 4s is low and background subtraction is difficult, we concentrate on the 4p shell. The electron spectrum shows a strong tail after the initial peak for the I 4p⁻¹ hole state in ICN, which suggests that it is strongly mixed with isoenergetic underlying states and continua, as in the analogous cases in Xe [10]. This characteristic of the 4p shell in iodine has been seen before in the photoelectron spectra of iodine compounds [14, 15] and in their X-ray emission [15], and was modelled there in terms of fluctuations in orbital character. In particular, the 4d⁻² double hole configuration should give rise to several levels close to or below the expected energy of 4p⁻¹ which, if populated, would be expected to decay to fourfold ionized products. In accordance with this, the dominant charge state after I 4p⁻¹ ionization is four, as deduced from the coincident mass spectrum and multiple ion coincidences (see Fig. 5 and Table 2). In the mass spectra (cf. Fig. 2 for 4p and Fig. 3 for 4s) the I⁺ ion almost vanishes, I²⁺ becomes strong, and I³⁺, N²⁺ and C²⁺ appear.

In order to find the relative intensities of the different decay pathways we again create an ion-ion coincidence map in correlation with the 4p photoelectrons, subtract accidental coincidences, do the same again in coincidence with an adjacent background section of the electron spectrum and after a second subtraction we obtain a map of the same sort as Fig. 4. The apparent relative intensities of processes producing two ions and one neutral atom with the photoelectron are read from this map, but are only apparent values because many or all of the detected ion pairs may originate from events producing ion triples, from which only two of the three ions were detected. To calculate the real fractions of ion pair decays we need the observed number of ion triples and the detection efficiencies for the undetected partner. These efficiencies can be estimated from the hollowness of the corresponding TOF peaks within the observed ion triples, together with the estimated collection efficiencies for thermal ions. The most abundant apparent pair in coincidence with I 4p⁻¹, for instance, is C⁺ + I²⁺, for which 2640 counts are recorded after background subtraction. Unless really involving a neutral N, these can come only from the ion triple, C⁺ + N⁺ + I²⁺, for which we see 467 detected counts. For the missing nitrogen ion, the best estimate of collection efficiency f_i is 0.2 ± 0.05 . With this estimate the residual count for the ion pair with neutral N is 354 ± 600 counts, which is compatible with zero. The same result of compatibility with zero real intensity is obtained for almost all the ion pair yields coincident with I 4p⁻¹, as shown italicised in Table 2. The only pairs which may have a real presence are those involving triply charged iodine atoms. For these there are no contributions from triples, because no triples with a total of five charges are observed, but the majority of raw ion pair counts as directly observed are in fact accidental or background coincidences whose correct subtraction is difficult.

For the events producing three ions in coincidence with the electrons we go through the same procedure, but also demand that to appear in the map two lighter ions must also be coincident with one of I⁺, I²⁺ or I³⁺ as well as the photoelectron. We assume that there are no charge separations where neutral iodine is produced. The raw map displaying ion pairs from I 4p⁻¹ coincident with I⁺ is shown as an example in Fig. 5; in this case subtraction of accidental coincidences and of the underlying background leaves the relative (but not absolute) intensities unchanged. In this context it is important that wide time limits are applied in the selection of the iodine ions, as the dissociations

from highly charged states often produce energetic ions with more flight time spread than the majority which make up the main peaks in the mass spectra. The effect is visible as skirts on the ion peaks in Figs. 2 and 3. The true relative intensities of the three-ion processes are then calculated by dividing peak areas by collection efficiencies, to obtain true intensities, from which the contributions of the three-ion events to apparent two-ion signals can be calculated as discussed above. The resulting relative intensities of the possible pathways are listed in Table 2, but it must be understood that these are subject to severe uncertainties because of the uncertainties of the ion collection efficiencies. The major conclusions seem clear, that fourfold ionization is the strongest decay channel with triple ionization second and double ionization very minor, if present. In triple ionization no neutral atom fragments or molecular fragments are evident, but the error limits are wide. It seems unlikely from these results that any neutral fragments are formed in 4-fold ionization.

Iodine 3d⁻¹

The photoelectron spectrum at 640 eV shows a single peak for 3d_{5/2} ionization but at 700 eV both the ²D_{5/2} and ²D_{3/2} levels stand out at 632 eV and 643 eV binding energy. The mass spectra and breakdown characteristics from the two levels are identical. Ionization from this shell produces another big change in the coincident mass spectrum (cf. Fig. 2) where more highly charged ions appear. Dissociation of highly charged precursors produces fragments with high kinetic energies, as is evident from details of the TOF spectra in Fig. 6 and also from the ion images. It is clear that a substantial fraction of the light fragment ions miss the ion detector, producing hollow peaks in the mass spectra. The loss of such ions makes accurate estimation of the overall collection efficiencies for them impossible. It is evident that the N⁺ and N²⁺ ions have higher kinetic energies than the C⁺ and C²⁺ congeners, so the effective collection efficiency is lowest for nitrogen. Only the iodine atomic ions have low enough energies to all fall on the sensitive area of the ion detector and so retain the same collection efficiency in all the measurements.

Although many ion pairs are recorded in coincidence with the 3d⁻¹ photoelectrons, the great majority, and probably all of them, are in fact the remnants of ion triples of which one component has been missed. Since the number of detected ion triples of each type is known (after all accidental and background subtractions) the expected number of pairs resulting from less than 100 % collection efficiency can be calculated if the efficiencies are known. In the cases where the (presumably) missing ion is an iodine atom, the calculation indicates that all observed pairs such as C⁺ + N⁺ are remnants of triples, within the experimental uncertainty. Where carbon or nitrogen ions are apparently missing the effective ion collection efficiencies are almost pure guesswork and no quantitative analysis has been attempted.

The abundances of the different ion triples in coincidence with I 3d photoelectrons, after all false coincidence subtractions, show the presence of initial charge states of the ICN molecule from 3 to 7, **in agreement with the results of Simon et al. [8]**. Their true relative abundances cannot be calculated without the unknown collection efficiencies, but as C and N ions are involved in every triple, the *relative* uncertainty is limited, probably to within a factor of two. The observed relative three-ion signals are listed in Table 3.

The most abundant degree of ionization is 4 (the same as with 4p initial ionization), and the next most abundant is five-fold ionization. This is the same ionization pattern as seen after 3d ionization of atomic Xe [8]. Within the breakdown patterns (see Table 3) we notice that of the light ions the most abundant products are C⁺ + N⁺ and if the charges are unequal C⁺ + N²⁺ is always more abundant than C²⁺ + N⁺.

Iodine 3p

Very extensive multiple ionization is evident from the mass spectrum coincident with I 3p photoelectrons. Possible analysis is limited by the extensive loss of light ions and the relatively few recorded events, but even from the mass spectrum it looks as though 6-fold ionization is the most abundant, on the basis that all events produce three ions. Six-fold ionization is indeed found to be most abundant among the detected ion triples, with 7-fold ionization a close second and 8-fold ionization also present. Among detected pairs in coincidence with $3p_{3/2}^{-1}$ the most abundant charge total is 5 with 6 a close second. If all the ion pairs are remnants of real triples it follows that the most probable missing charge is 1; the relative abundances of pairs and triples indicate that the collection efficiencies for the light ions are about 10 % on average, which seems reasonable. The lowest degree of ionization seen among detected triples is 4 and the highest with appreciable abundance is 8-fold (some 9-fold is seen too). As will be seen below, the occurrence of 8-fold ionization is supported by the kinetic energies carried by iodine ions, determined from the VMI images.

The mechanism of the 6- and 7-fold ionization must be Auger cascades, involving the iodine atom alone before the delocalised valence electrons contribute. The 3p hole is most likely filled initially by fast Coster-Kronig decay leaving a double hole in 3d and overall charge 2 as confirmed by the electron spectrum at 1040 eV. Two single Auger steps involving valence electrons would lead to 4-fold ionization, but the 10 4d or overall 18 $n=4$ electrons on the iodine atom itself are more likely to participate. If two double holes are produced in the $n=4$ shell and each decays by two sequential single Auger steps the final charge state will be 6. Additional cascades from 4s to 4p or 4p to 4d or double Auger decay at any stage will raise the final charges to 7 and 8 as observed.

Ion kinetic energies and angular distributions

Because the focus conditions in this experiment were set for VMI operation, TOF deviations in the spectra bear a complex and potentially ambiguous relationship to the initial on-axis momenta (energies and angles) of the fragment ions, so we concentrate instead on the ion images. Of the ion images recorded at the position-sensitive detector, only those of I^{n+} ions and CN^+ are complete. Some, or at high energies most of the lighter ions C^{n+} and N^{n+} miss the detector. But the I^+ and CN^+ ions formed at the lowest energies provide a starting point and allow the relationship between diameter of the ion rings and the ion energy to be calibrated by comparison with the kinetic energy releases determined in double ionization at EUV photon energies. In the work with He resonance radiation [6] the energy release in formation of $I^+ + CN^+$ was found to increase steadily with the available excess energy deposited in the precursor doubly charged molecule. In double ionization by the Auger process after formation of a 4d hole, we can estimate the excess energy by examination of the Auger spectra coincident with the $4d_{5/2}$ and $4d_{3/2}$ photoelectron lines and with the CN^+ fragment (assuming this is always formed with I^+). The Auger spectrum obtained in coincidence with doubly charged products (see Fig. 7) might be expected to differ from the double ionization spectra obtained in photoionization, particularly because triplet states are prominent in photoionization but almost completely absent in Auger spectra [16]. In fact very little difference is detected at the present resolution, perhaps because spin-orbit coupling in iodine is strong and mixes the singlet and triplet states.

In Ref. [6] it is shown that in photoionization, for ionization energies between 30.5 and about 40 eV the most probable products are the $I^+ + CN^+$ pair with a mean total kinetic energy release of about 5.5 eV. At higher energies up to 40 eV the main products are $I^+ + C^+ + N$, formed by

fragmentation of intermediate CN^+ , and $\text{I}^{2+} + \text{CN}$. The ion pair $\text{I}^+ + \text{N}^+$ is not formed appreciably with 40.8 eV photon energy, but as it is abundant in the spectrum coincident with $4d^{-1}$, it must be formed at ionization energies above 21 eV. The Auger spectrum produced by decay of a $4d$ hole (cf. Fig. 7) and the complementary fragmentation diagrams confirms this, and also show that the two-body products $\text{I}^+ + \text{CN}^+$ are formed in the same ionization energy range, and thus with the same initial internal energy, in Auger decay as in photoionization. These threefold and fourfold coincidence measurements extend the fragmentation diagram of Ref. [6] and agree with it in the range where they overlap.

Since the internal energy range where the two-body products are formed is the same in photoionization and Auger decay from $4d^{-1}$, the relationship between radii of ion rings in the present VMI images and the kinetic energies can be calibrated by comparison with the earlier photoionization data. For a two-body decay forming $m_1^{z1} + m_2^{z2}$ with the radius R_1 for ion 1 is formally

$$R_1 = k\{Um_2/z_1(m_1+m_2)\}^{1/2}$$

Here k is a constant including fixed apparatus parameters such as dimensions and the strengths of applied electric fields and U is the total CM kinetic energy release. If U is identified with the Coulomb repulsion energy $z_1z_2e^2/r_{12}$ for ions at the effective distance r_{12} where charge separation takes place, then the radius of the ring for a given ion depends only on the mass and charge of the counter-ion, not on the charge of the ion actually observed, i.e.

$$R_1 = k\{e^2/r_{12}\}^{1/2}\{m_2z_2/(m_1+m_2)\}^{1/2}$$

The maximum radius of the ring for I^+ ions coincident with $\text{I } 4d_{5/2}^{-1}$ is 11.5 mm, as shown in Fig. 5. Using 5.5 eV as the estimated CM kinetic energy release, of which 0.9 eV is carried by the I^+ ion, we derive $k = 11.9 \text{ mm eV}^{-1/2}$ in terms of the energy of the observed ion; the radius of the ring for CN^+ gives the same value within the experimental uncertainty.

Using this calibration, it is interesting to examine the rings for iodine ions in coincidence with the $\text{I } 4p$ photoelectron line, where production of two charged particles is still apparent but actually arises from partial observation of the dominant three-ion channels (see Table 2). The image for the I^+ ion is very weak, but the image for the I^{2+} ion, Fig. 6, is clear and shows a maximum radius of 16 mm. If the inter-charge distance is taken to be fixed by the molecular geometry, this implies that the counter-ion(s) have double the charge observed in $4d$ Auger decay ($11.5\sqrt{2} = 16.3$). This agrees very well with the relative abundances in Table 2, where $\text{I}^{2+} + \text{C}^+ + \text{N}^+$ is by far the most intense channel. At the highest photon energies, some iodine ions appear as rings with radii of 20 to 25 mm. For the I^{4+} ions formed at a photon energy of 945 eV, for instance, the outermost distinct ring edge is at 24 mm, implying according to the same logic that the counter-ions carry a total of four more positive charges. This suggests that at this photon energy formation of holes in the $3p$ shell is significant, as this is the shell whose ionization produces I^{4+} in abundance and very likely, by analogy with Xe [10], leads to overall 8-fold ionization. The agreement of the apparent I^{n+} ion energies with this simple model suggests that the initial process is always I-C bond breaking with well-developed charges on both iodine and on a short-lived CN ion complex which subsequently breaks up, as in the process demonstrated in double ionization [6].

None of the ion images observed at the different photon energies shows any angular anisotropy in the LAB frame, so there is no favoured angular distribution relative to the light's polarisation or propagation vector. The angular distributions of one ion relative to another are highly structured, but because of ion losses we can rely upon them only at the very lowest ionization energies, i.e. from $\text{I } 4d$ ionization. For the two-body pair $\text{I}^+ + \text{CN}^+$ the 180 degree separation required

by momentum conservation is clearly observed. For ion pairs $I^+ + C^+$ and $I^+ + N^+$ where the third partner is neutral the angular spread about a mean of 180 degrees clearly denotes that some momentum is carried by the neutral atom. Because the VMI image is a projection of the full 3-D Newton sphere onto the plane of the detector, we cannot use it alone to determine the true initial CM momentum vectors of the particles. To approach that, analysis of the TOF distribution and their correlations is also essential to provide the third dimension.

Conclusions

Initial hole production in the 1s shells of carbon or nitrogen or in the 4d shell of iodine in ICN produces mainly double ionization, a hole in I 4p or I 4s produces mainly fourfold ionization, one in 3d also produces mainly fourfold and fivefold ionization while a hole in 3p results in six-fold and higher ionization. The present results are consistent with the idea that when ICN is ionized to have equal numbers of charges and atoms (ICN^{3+}), some subsequent decays still produce neutral fragments but few or no molecular fragments. When it is ionized to ICN^{4+} , with more charges than atoms, very few or no neutral fragments are formed. Higher degrees of ionization produce complete atomization with all fragments charged. In addition to these physical conclusions, the difficulty and ambiguities of the present analysis demonstrate that to make effective advances in this investigation we need higher collection efficiencies, particularly for light ions, and longer run times to gather better statistics. Until this is achieved, and product ion momenta are also determined by complete VMI and TOF analysis it seems premature to attempt a full theoretical description of the decays from hole states in each inner shell. A kinetic model would require a very large number of unknown rate parameters for the decay processes and charge transfers, but we note that Fukuzawa *et al.* [17] have made advances in this direction with a Monte-Carlo approach and Motomura *et al.* [18] have applied a simpler parametric model to the related case of Coulomb explosion by multiphoton ionization using an X-ray free-electron laser.

Acknowledgements

This work has been financially supported by the Swedish Research Council (VR) and the Knut and Alice Wallenberg Foundation, Sweden. We thank the Helmholtz Zentrum Berlin for the allocation of synchrotron radiation beam time and the staff of BESSY-II for particularly smooth running of the storage ring in top-up mode during the single-bunch runtime. The research leading to these results has received financial support from the European Community's Seventh Framework Programme (FP7/2007-2013) under grant agreement no. 312284 and from the Helmholtz Zentrum Berlin. J.P., C.S.S. and M.B. acknowledge the support of the UK EPSRC *via* Programme Grant EP/L005913/1.

References

- [1] T. A. Carlson and R.M. White, *J. Chem. Phys.* **44**, 4510 (1966).
- [2] J.S. Wright *et al.*, *Phys. Rev. A* **59**, 4512 (1999).
- [3] K. Kwon and A. Moscowitz, *Phys. Rev. Lett.* **77**, 1238 (1996).
- [4] T. Kitamura *et al.*, *J. Chem. Phys.* **115**, 5 (2001).
- [5] M. Pitzer *et al.*, *Science* **341**, 1096 (2013).
- [6] J.H.D. Eland and R. Feifel, *Chem. Phys.* **327**, 85 (2006).
- [7] J.H.D. Eland, *Chem. Phys. Lett.* **203**, 353 (1993).
- [8] M. Simon, M. Lavollée, M. Meyer and P. Morin, *Journal de Chimie Physique et de Physico-chimie Biologique*, **90**, 1325 (1993).
- [9] S. Plogmaker *et al.*, *Rev. Sci. Instrum.* **83**, 03115 (2012).

- [10] J.H.D. Eland *et al.*, *J. Phys. B: At. Mol. Opt. Phys.* **48**, 205001 (2015).
- [11] A.T.J.B. Eppink and D.H. Parker, *Rev. Sci. Instrum.* **68**, 3477 (1997).
- [12] http://www.roentdek.com/info/Delay_Line/
- [13] A. Hult-Roos *et al.*, submitted for publication.
- [14] U. Gelius, *J. Electron Spectrosc. Rel. Phenom.* **5**, 985 (1974).
- [15] M. Ohno, *Physica Scripta* **21**, 589 (1980).
- [16] H. Ågren, *J. Chem. Phys.* **75**, 1267 (1981) (Appendix B).
- [17] H. Fukuzawa *et al.*, *Phys. Rev. Lett.* **110** 173005 (2013).
- [18] K. Motomura *et al.*, *J. Phys. Chem. Lett.* **6** 2944 (2015).

Table 1. Relative strengths of competing decays from ICN^+ ($I\ 4d^{-1}$, 59 eV).

Channel	Threshold*	Intensity ($\Sigma = 1000$)	HeII (48.4 eV) [6b]
ICN^{2+}	29 eV	21	
$\text{CN}^+ + \text{I}^+$	27.8 eV	276	100
$\text{N}^+ + \text{IC}^+$	ca. 30 eV	9	4
$\text{C} + \text{N}^+ + \text{I}^+$	33 eV	254	23
$\text{C}^+ + \text{N} + \text{I}^+$	33 eV	354	49
$\text{C} + \text{N} + \text{I}^{2+}$	35 eV	77	
$\text{CN}^+ + \text{I}^{2+}$	47 eV	18	
$\text{C}^+ + \text{N}^+ + \text{I}^+$	47 eV	5	3
$\text{C}^+ \text{ or } \text{N}^+ + \text{I}^{2+}$	52 eV	4	

*Thermodynamic thresholds given in the tables are for products formed with zero kinetic energy or internal energy. Actual onsets will include at least a minimum kinetic energy, which can be estimated as 3.5 eV for two singly charged fragments, 7 eV for one doubly charged and one singly charged, 14 eV if both are doubly charged.

Table 2. Relative strengths of decay channels from ICN^+ ($4p^{-1}$, 132 eV).

Channel	Threshold*	Relative intensity ($\Sigma = 100$)
$\text{C} + \text{N}^+ + \text{I}^+$	33 eV + KER	-3 ± 6
$\text{C}^+ + \text{N} + \text{I}^+$	33 eV + KER	3 ± 6
$\text{C}^+ + \text{N}^+ + \text{I}^+$	47 eV + KER	16 ± 3
$\text{C}^+ + \text{N} + \text{I}^{2+}$	52 eV + KER	12 ± 20
$\text{C} + \text{N}^+ + \text{I}^{2+}$	52 eV + KER	-1 ± 3
$\text{C}^+ + \text{N}^+ + \text{I}^{2+}$	67 eV + KER	61 ± 3
$\text{C}^{2+} + \text{N}^+ + \text{I}^+$	71 eV + KER	6 ± 1
$\text{C}^+ + \text{N}^{2+} + \text{I}^+$	76 eV + KER	8 ± 2
$\text{C} + \text{N}^+ + \text{I}^{3+}$	76 eV + KER	3 ± 4
$\text{C}^+ + \text{N} + \text{I}^{3+}$	76 eV + KER	3 ± 2

Table 3. Apparent relative intensities ($\Sigma=100$) of ion triples coincident with $I\ 3d^{-1}$ ionization.

With:	I^+	I^{2+}	I^{3+}	I^{4+}
$\text{C}^+ + \text{N}^+$	9	42	11	2

$C^{2+} + N^+$	3	2	2	-
$C^+ + N^{2+}$	7	8	9	2
$C^{2+} + N^{2+}$	-	1	2	-

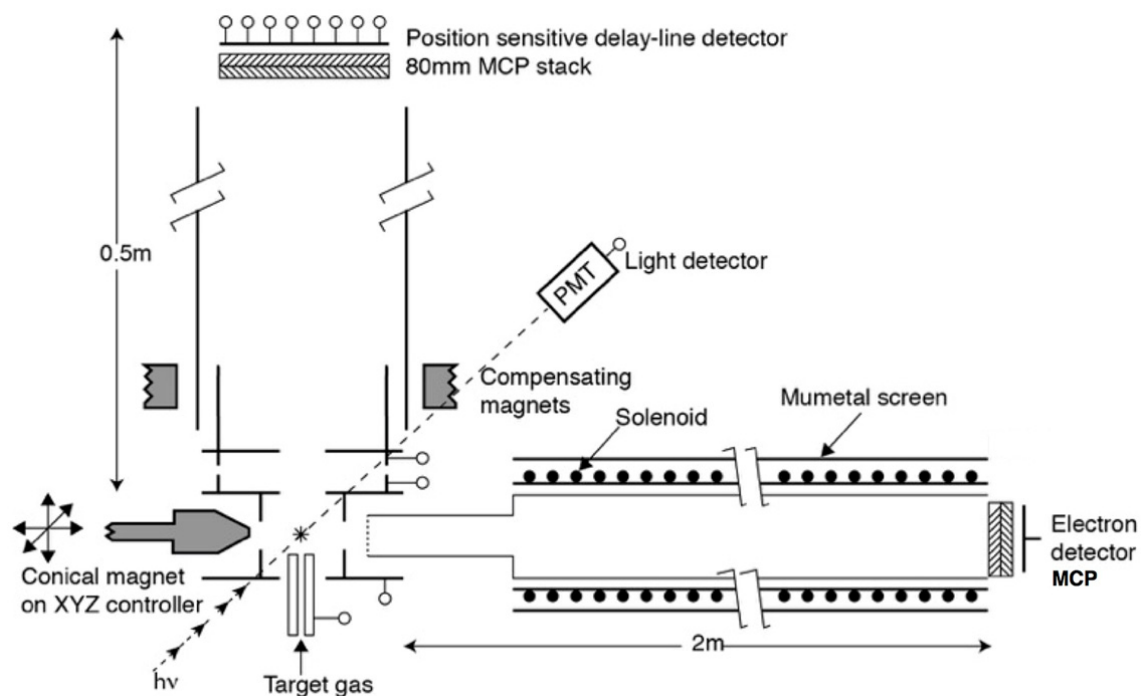


Figure 1. The magnetic bottle TOF electron spectrometer and perpendicularly mounted VMI mass spectrometer for photoions. The electrodes around the source region are pulsed to send ions into the mass spectrometer at about 30 ns after a light pulse, when all important photoelectrons have safely entered the field-free flight tube.

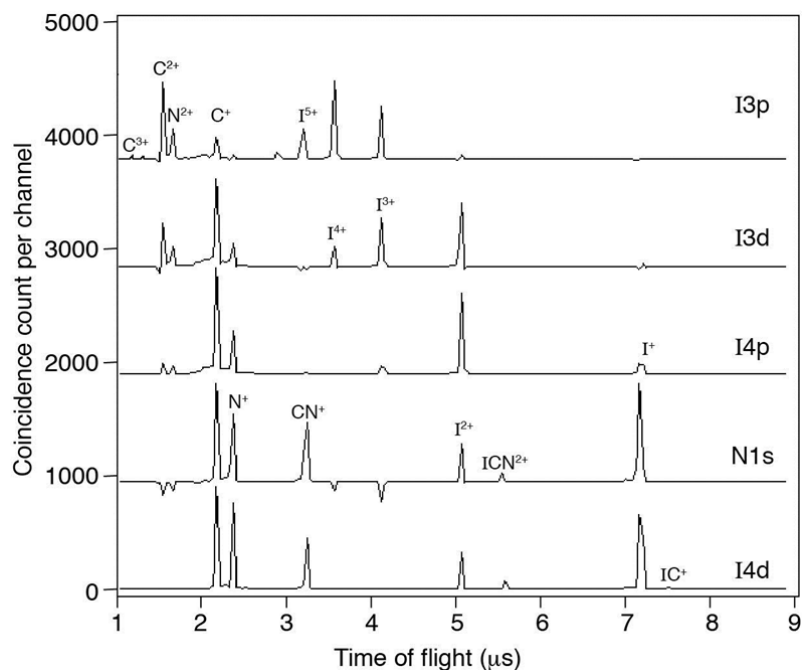


Figure 2. Mass spectra coincident with the different photoelectrons indicated, measured at beamline U49/2-PGM-2 with diminished sensitivity for heavier ions. Accidental and background false coincidences have been subtracted.

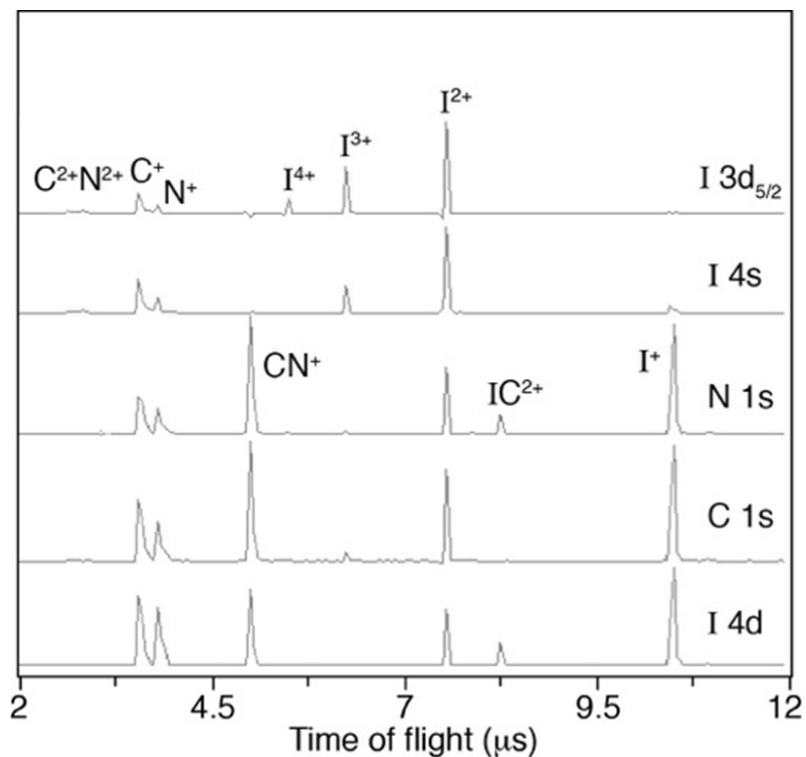


Figure 3. Mass spectra coincident with selected photoelectron lines taken at beamline U52-SGM, with improved sensitivity for heavier ions. The spectra with I 4d, I 4s, C 1s and N 1s were extracted from data at 350 eV photon energy. The spectrum with I 3d_{5/2} was taken from the 700 eV data. Comparison with the spectra in Fig. 2 from the I 4d, I 3d and N 1s shells illustrates the effect of improved sensitivity to heavier ions.

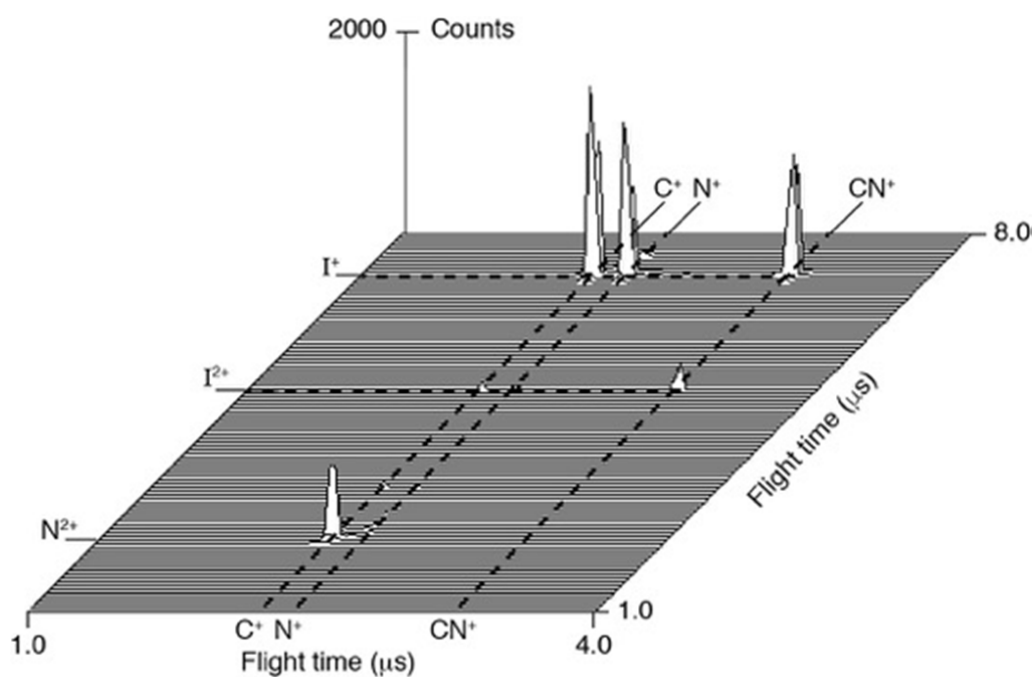


Figure 4. Isometric projection of the coincidence map of ion pairs coincident with the 4d photoelectron line after all false coincidence subtractions.

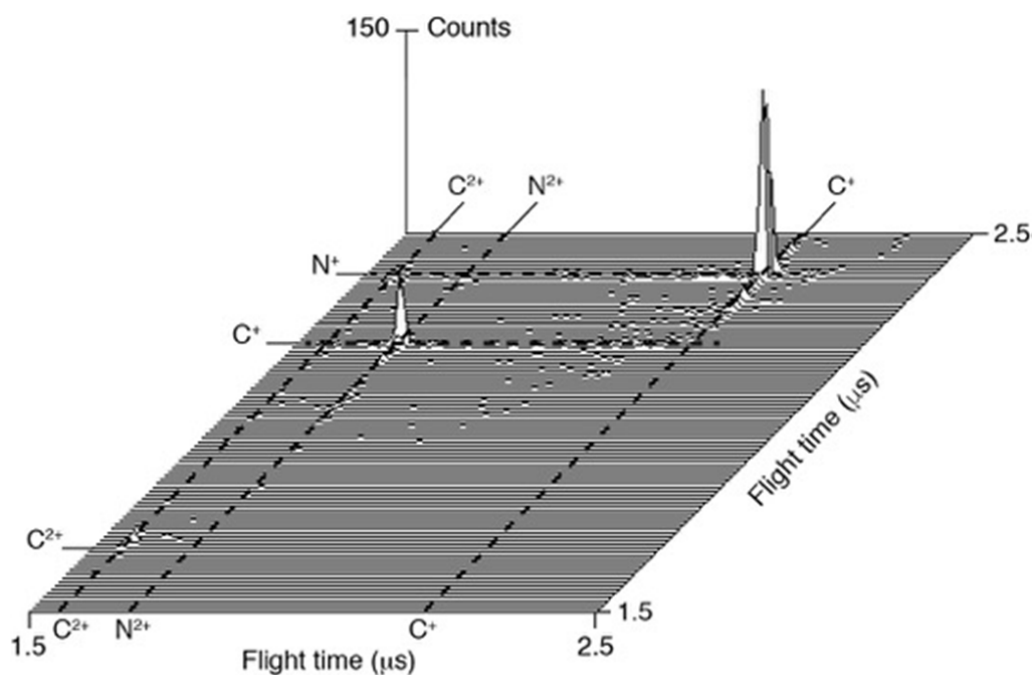


Figure 5. Isometric projection of the map of ion pairs also coincident with the I^{+} ion as well as the 4p photoelectron. Background coincidences have not been subtracted, but their removal does not change the relative peak intensities.

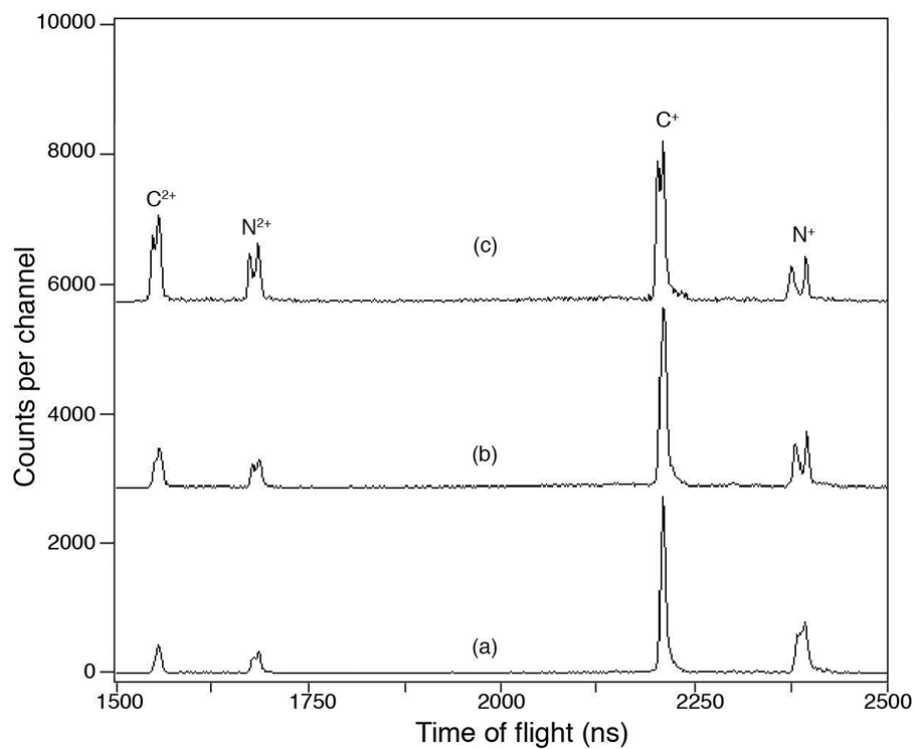


Figure 6. Detail of some TOF mass spectra showing the effect of high kinetic energies on the low mass peak shapes. (a) Ions coincident with I^{+} at 945 eV where $3d^{-1}$ ionization is dominant. (b) Ions coincident with I^{2+} at 945 eV. (c) Ions coincident with I^{4+} at 1200 eV.

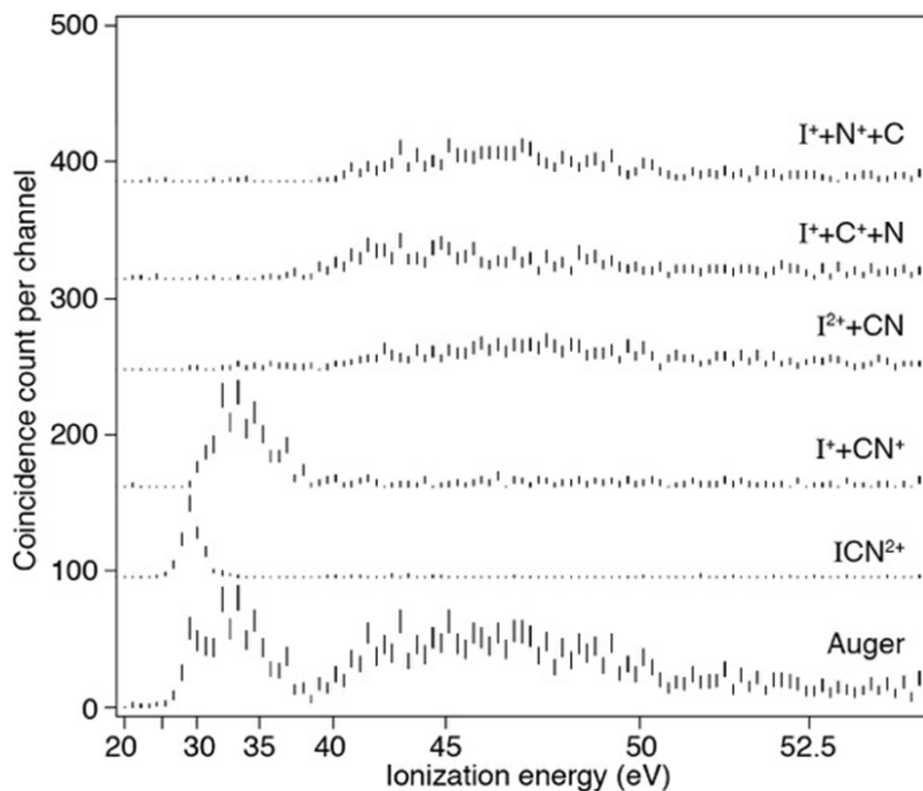


Figure 7. Partial Auger electron spectra coincident with doubly charged products following production of a 4d hole on iodine at 110 eV photon energy, **together with their sum, which is indistinguishable in shape from the overall Auger spectrum.** The energy scale is non-linear because the raw data is linear in time and there are too few counts to allow a sensible conversion to a linear energy scale. The intensity scale is approximately common to all, but the data have been displaced upwards for display.

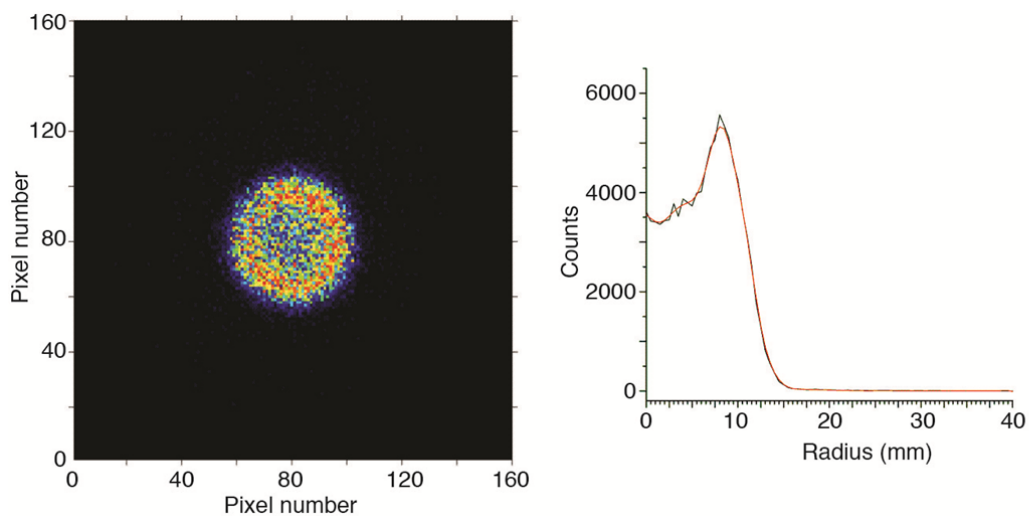


Figure 8. The I^+ image coincident with the $4d_{5/2}$ photoelectron line in ICN at 110 eV photon energy and its radial intensity distribution. As a measure of the outside radius of the image we take the point at half height on the descending slope.

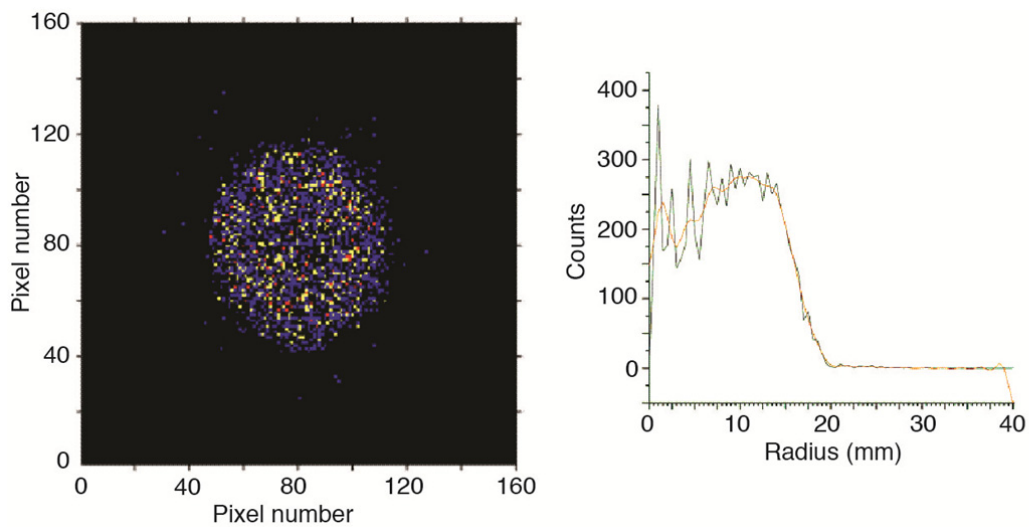


Figure 9. Image for I^{2+} coincident with the 4p photoelectron line at 200 eV photon energy. The red line through the radial intensity distribution is the result of smoothing.

